

Photoelectrochemical Characterization of CuInSe₂ and Cu(In_{1-x}Ga_x)Se₂ Thin Films for Solar Cells

Heechang Ye,[†] Hyun S. Park,[†] Vahid A. Akhavan,[‡] Brian W. Goodfellow,[‡] Matthew G. Panthani,[‡] Brian A. Korgel,[‡] and Allen J. Bard^{*†}

Center for Electrochemistry, Department of Chemistry and Biochemistry, The University of Texas at Austin, Austin, Texas 78712, United States, Department of Chemical Engineering, Texas Materials Institute, and Center for Nano- and Molecular Science and Technology, The University of Texas at Austin, Austin, Texas 78712-1062, United States

Received: August 27, 2010; Revised Manuscript Received: November 17, 2010

Photoelectrochemical (PEC) studies of CuInSe₂ (CIS) and Cu(In_{1-x}Ga_x)Se₂ (CIGS) thin films prepared by electrodeposition and spray coating of nanocrystals were carried out. PEC reductions of methyl viologen (MV) in aqueous solution and ethyl viologen (EV) in acetonitrile were used to evaluate the thin-film performance by measuring the photocurrent. Deposition of a CdS layer on CIS and CIGS films strongly enhanced the photocurrent; for example, a nanocrystal-CIS film showed about 100 times higher photocurrent with a thin CdS layer. Capacitance measurements and Mott–Schottky plots were obtained to find the flat band potential. Incident photon to current conversion efficiencies (IPCE) and absorbed photon to current conversion efficiencies (APCE) obtained from PEC measurements were about 20% and 40–70%, respectively.

Introduction

We report the photoelectrochemical (PEC) characterization of CuInSe₂ (CIS) and Cu(In_{1-x}Ga_x)Se₂ (CIGS) thin films deposited by electrodeposition and nanoparticle spray. There has been much recent interest in producing efficient CIS and CIGS thin films for solar photovoltaic (PV) cells because such inorganic thin film based devices can show high efficiencies and lower cost than single crystal Si solar cells. However, these CIS and CIGS thin films are currently produced by vacuum deposition processes, and there has been much interest in replacing this with lower cost processes, such as electrochemical deposition and the synthesis of nanoparticles (NPs) to produce inks.^{1–6} The quality of the films produced by these new approaches is usually assessed by fabricating complete PV cells, a process that involves sequential deposition of CdS, ZnO, and transparent conductive layers followed by deposition of a metal collection grid. This is difficult and time-consuming leading to a long optimization period to find optimum materials. Testing of the films in a PEC cell is faster and allows one to assess the CIS or CIGS material independent of problems such as interface contact with the full device architecture because the appropriate liquid electrolyte can form a reproducible contact. We discuss here PEC studies of CIS and CIGS films by different NP synthesis methods and by electrodeposition.

There have been several other PEC studies of CIS and CIGS thin films.^{7–11} Most of these focused on the hydrogen evolution reaction (HER) on the p-type CIS and CIGS films as related to PEC water reduction. However, the HER is not the most appropriate electrochemical reaction for PEC characterization of the quality of CIS and CIGS films because the HER is a complex inner sphere reaction that requires either significant

overpotentials or a suitable electrocatalyst. In the absence of a surface electrocatalyst, the rate of the HER is affected not only by the light absorption and electron–hole separation/recombination properties of the material but also by the electrocatalytic property of films. Moreover, the HER is carried out in an aqueous solution in which CIS and CIGS film surface may be unstable in long-term experiments.

Here, we demonstrate a PEC study of CIS and CIGS films prepared by electrodeposition and nanoparticle spray using the ethyl viologen (EV) or methyl viologen (MV) reduction reactions in acetonitrile (MeCN) and water solution, respectively. This method can evaluate material properties even when the films are somewhat porous, whereas solid-state full devices would be affected by leakage current. Moreover, we report that CIS and CIGS films with a layer of CdS show much higher photocurrent because of suppression of recombination processes by the CdS layer.

Experimental Section

Preparation of CIS and CIGS Films. CIS and CIGS films were prepared using two approaches: (1) electrochemical deposition of CIGS and (2) spray coating of nanoparticle-CIS (NP-CIS) and CIGS.

Electrochemical Deposition of CIGS. The preparation of CIGS precursor solution and its deposition potential were based on the method by Calixto et al.¹² The precursor solution consists of CuCl₂·2H₂O (99.995%), InCl₃ (98%), GaCl₃ (99.999%), and H₂SeO₃ (98%) with LiCl (99%) as a supporting electrolyte in deionized (DI) water. All chemicals were purchased from Sigma-Aldrich and were used as received. The final concentrations of CuCl₂, InCl₃, GaCl₃, H₂SeO₃, and LiCl in the solution were 2.56, 2.40, 5.70, 5.46, and 240 mM, respectively. After the precursor solution was prepared, pH 3 buffer powder (Hydriion pH 3.00 ± 0.02, Fluka) was added. The resulting solution had pH 2.3–2.4. An AC sputtered molybdenum thin film (1 μm) on a glass substrate was used as the working electrode. The Mo working electrode was sonicated in detergent

* To whom correspondence should be addressed. E-mail: ajbard@mail.utexas.edu.

[†] Department of Chemistry and Biochemistry, The University of Texas at Austin.

[‡] Texas Materials Institute and Center for Nano- and Molecular Science and Technology, The University of Texas at Austin.

(Contrex, Decon), ethyl alcohol (99.5%, Pharmco-Aaper), and DI water for 5 min each before the deposition. A Pt counter electrode and a Ag/AgCl reference electrode were used to complete the three-electrode configuration. The deposition was conducted on a vertically dipped working electrode in magnetically stirred solution at room temperature. Solution volume for deposition was 200 mL with the working electrode area of 2.3 cm². The deposition was conducted at a controlled potential of -0.46 V versus Ag/AgCl for a deposition charge of 1.4 C/cm² and then at -0.56 V for 5.6 C/cm². The electrodeposited CIGS film was then annealed under a selenium atmosphere at 430 °C for 20 min with 0.36 g of Se powder (99.99%, Aldrich) placed in the same quartz boat with the film. The ramp rate for annealing was 20 °C/min, and the actual temperature overshot to 500 °C during the selenization. Then, the annealed film was etched with 0.1 M KCN solution for 1 min at 55 °C. The film was thoroughly rinsed with DI water after the etching. The CdS layer was deposited on the etched CIGS film by the chemical bath deposition (CBD) method.¹³ The bath solution consisted of 1.5 mM CdSO₄·8/3H₂O (98%, Fisher), 7.5 mM (NH₂)₂CS (99%, Alfa-Aesar), and 1.5 M NH₄OH (Fisher). The CIGS film was immersed into the bath solution for 16 min at the solution temperature of 60 °C. The film was rinsed with DI water after the deposition of CdS. The resulting film was characterized by X-ray diffraction (XRD) and energy-dispersive spectroscopy (EDS) to investigate crystal structure and elemental composition (see Supporting Information).

Spray Deposition of NP-CIS. CIS nanocrystal-based films were deposited by spraying a dispersion (i.e., an ink) of CIS nanocrystals in toluene onto a working electrode under ambient conditions. Nanocrystal ink syntheses have been outlined elsewhere.⁵ The specific nanoparticle-based ink formulation used here was different depending on whether or not the particles were to be selenized.

CIS nanoparticles for selenization were synthesized as previously reported⁵ with slight modification. In a 100 mL three-neck flask (flask 1), 10 mmol CuCl (0.998 g, 99.995%, Aldrich), 10 mmol of InCl₃ (2.21 g, anhydrous 99.99%, Aldrich), and 20 mmol elemental Se powder (1.58 g, 99.999%, Aldrich) were combined in a nitrogen-filled glovebox. The flask was removed from the glovebox, was attached to a Schlenk line, and was placed on a heating mantle. In a separate 50 mL one-neck flask (flask 2) attached to a Schlenk line, 50 mL of oleylamine (>70%, Aldrich) was degassed and was dried at 110 °C for 1 h under 300 mTorr of vacuum and then was purged with nitrogen for 10 min. The oleylamine in flask 2 was then added to the reactant mixture via cannula transfer. The mixture was then ramped to 200 °C and was held for 30 min. The mixture was then quickly ramped to 260 °C and was allowed to react for 10 min. The heating mantle was then removed, and the flask was allowed to cool to room temperature.

CIS and CIGS nanoparticles not for selenization were synthesized by a slightly modified procedure. Briefly, 5 mmol of CuCl and 5 mmol of a combination of InCl₃ and GaCl₃ were combined in a three-neck flask in an oxygen-free environment in a glovebox with 50 mL of oleylamine (>70%, Sigma-Aldrich). The reaction vessel was sealed with a septum and was mounted on a conventional Schlenk line setup outside the glovebox. The reactants were placed under vacuum at 110 °C for 30 min to remove any residual oxygen and water, and then the reaction vessel was purged with pure nitrogen for 30 min. At this stage, the temperature of the reaction vessel was raised to 240 °C, and 10 mL of a 1 M TBP:Se (0.79 g selenium powder dissolved in 10 mL of tributylphosphine) solution prepared

previously in the glovebox was injected into the reaction vessel. The temperature was maintained for 10 min; then, the heating mantle was removed and the reaction was allowed to cool to room temperature.

In both cases, the CIS nanocrystals were washed and purified after the synthesis. The cooled reaction product was poured into a glass centrifuge tube with 10 mL of ethanol. The solid product was separated by centrifugation at 4000 rpm for 1 min. The supernatant was discarded, and the product was redispersed in 5 mL of toluene. The solution was centrifuged again at 4000 rpm for 1 min to remove any larger, poorly capped products; the supernatant was poured into a new centrifuge tube, and the solid precipitate was discarded. Ethanol was added dropwise to the solution until a slightly turbid dispersion was achieved. The dispersion was then centrifuged at 4000 rpm for 1 min to precipitate the nanocrystal product. The supernatant was discarded, and the precipitate was redispersed in toluene. Again, a minimal amount of ethanol was added, and the dispersion was centrifuged one last time. The supernatant was discarded, and the precipitate was redispersed in toluene at a concentration of 20 mg/mL.

The resulting dispersion was sprayed from an Iwata airbrush (Eclipse HP-CS) with a 50 psig head pressure. Several different back contact electrodes (Au, Mo, Ni, or ITO) could be used for deposition of the nanoparticle films. Most of the work was done on 60 nm of thermally deposited Au on glass substrate having 5 nm of Cr as an adhesion layer between Au and glass, while the selenized or heat-treated films were prepared on Mo substrates as used in the electrodeposition to avoid possible diffusion of Au into CIS and CIGS films during heat treatment and destruction of the Au layer at high temperatures. Nanocrystal films that were to be selenized were sprayed in three stages with a 10 min bake at 150 °C on a hot plate between consecutive nanocrystal depositions. This allowed for the deposition of thicker films (about 1 μm) without the formation of many cracks that penetrate the entire film.

In some cases, CIS nanocrystal films were annealed under a Se rich atmosphere (selenization) to achieve large micrometer-sized grains of CIS. The selenization was performed in a Thermolyne F79500 three-zone tube furnace with a quartz tube (5 cm diameter, 120 cm length) under a flow of nitrogen gas. A quartz boat containing 5 g of Se pellets (<4 mm, 99.99+%, Aldrich) was placed in the center of the first zone (most upstream). The nanocrystal films on Mo coated glass substrates were placed into another quartz boat, which was then placed into the center of the second zone of the furnace. The tube was then connected to the nitrogen stream and was purged at a rate of 2 L/min for 20 min. After purging, the gas flow rate was reduced to 0.02 L/min, and the temperature of zone 1 was raised to 335 °C while zone 2 was raised to 400 °C. These temperatures were held for 30 min in order to melt the Se pellets and to burn off the organic ligands in the nanocrystal film. The temperature of zone 1 was then increased to 615 °C and zone 2 was increased to 550 °C. These temperatures were maintained for 60 min. After this, the power to the heating elements was turned off and the lid to the furnace was opened. This cooled the walls of the tube so that Se vapor condensed on the walls of the tube rather than on the samples. Also, the gas flow rate was increased to compensate for the decrease in pressure inside the tube as it cooled. Once the furnace had cooled to room temperature, the samples were removed from the tube furnace and were stored in a nitrogen-filled glovebox.

Further processing of some nanocrystal films involved deposition of a thin layer of CdS based on a modified CBD

method.¹⁴ Nanocrystal films were preheated to 90 °C for 5 min. A 0.7 mL solution of 3 mM CdSO₄, 0.53 M (NH₂)₂CS, and 8.1 M NH₃ in water was drop cast onto the surface of the nanoparticle film. The reaction chamber was quickly sealed by placing an inverted Petri dish directly over the surface. The reaction was allowed to proceed for 2 min. The substrate was removed from the heating plate, and the surface was washed with DI water.

Photoelectrochemistry. The CIS and CIGS thin films deposited on Au/glass or Mo/glass substrates were used as photoelectrodes. The geometric area of the electrode exposed to electrolyte solution and light irradiation using an O-ring was 0.2 cm². All electrochemical experiments were carried out in a borosilicate glass cell using a three-electrode configuration with a Pt-gauze counter electrode and a Ag wire (MeCN experiments) or a Ag/AgCl (aqueous experiments) reference electrode. The potential of the Ag wire reference electrode was calibrated using the ferrocene/ferrocenium (Fc/Fc⁺) redox couple, and all potentials reported here were converted versus the normal hydrogen electrode (NHE) unless otherwise specified. Light irradiation was performed using a Xe lamp (Oriel, 150 W) with a light intensity of about 100 mW/cm² after considering some loss from the light absorption through the electrolyte solution and the glass cell. A monochromator (Oriel) was used in combination with a power meter and a silicon detector (Newport) to measure the light flux for calculation of incident photon to current conversion efficiencies (IPCE). A potentiostat (CH Instruments, Austin, TX) equipped with a PC computer was used for electrochemical measurements. Electrochemical solutions were prepared either in MeCN (Sigma-Aldrich) or DI water with tetrabutylammonium hexafluorophosphate (TBAPF₆, Sigma-Aldrich) and 0.1 M KCl (Fisher) as electrolytes, respectively. The 0.1 M ethyl viologen doperchlorate (EV(CIO₄)₂) (MeCN) and methyl viologen dichloride (MVCl₂) (water) were dissolved in solution as redox species. Electrochemical impedance spectroscopy (EIS) was performed using a Solartron 1250/1286 frequency response analyzer and electrochemical interface system. Impedance spectroscopy was carried out in electrolyte-only solutions using frequencies of 250, 500, and 1000 Hz and an AC amplitude of 10 mV at each potential.

Results and Discussion

Photoelectrochemical Measurement of CIS and CIGS Films. In a PEC system, an appropriate redox couple dissolved in electrolyte solution is used as the electron or hole acceptor in place of a metal or semiconductor contact. By obtaining the current–potential behavior with respect to a standard reference electrode in the dark and under illumination, information about the energies of the valence and conduction bands and the efficiency of the conversion of incident photons to useful photocurrent can be obtained. In general for p-type semiconductors, electrons are transferred from the conduction band to the solution-phase oxidant and electrons are transferred from the back ohmic contact into the semiconductor, and so the observed current is reductive (cathodic) as described in many studies and reviews.¹⁵

There are several requirements for a suitable redox couple: (1) The standard reduction potential should be energetically below the conduction band edge for photoreduction meaning that the reduction potential should lie within the band gap of the CIS or CIGS material. (2) The solubility should be sufficiently high in the electrolyte solution so that the current is not limited by mass transfer of the oxidant to the semiconductor surface and the measured photocurrent is only limited by

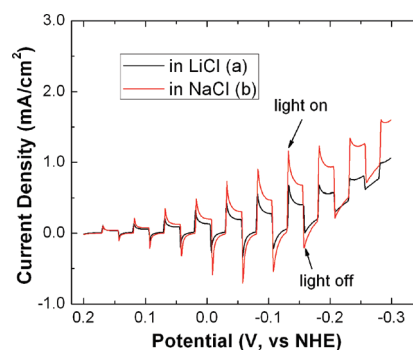


Figure 1. Linear sweep voltammograms (LSVs) of electrodeposited-CIGS films on Mo with light chopping in 0.1 M EV(CIO₄)₂ and 0.1 M TBAPF₆ in MeCN. Scan rate: 10 mV/s, light source: Xe lamp (ca. 100 mW/cm²). Electrodeposition was performed in LiCl electrolyte (a, black) and NaCl (b, red).

the photogenerated electron flux to the surface. (3) The solution should not absorb significant amounts of the light because the semiconductor is usually irradiated through the solution. (4) The kinetics of the redox reaction should be fast so that electron transfer can occur without appreciable overpotential (unlike the proton reduction reaction used for some PEC studies of CIS and CIGS films).^{7–11} (5) The solvent and redox couple should be selected to avoid photoinduced decomposition of the semiconductor. According to the above requirements, EV²⁺/EV⁺ and MV²⁺/MV⁺ were selected as redox couples for electrochemical studies of CIS and CIGS films in aqueous and MeCN solutions, respectively.

Figure 1 shows the linear sweep voltammograms (LSVs) of an electrodeposited-CIGS film (ED-CIGS) on a Mo substrate in a 0.1 M EV(CIO₄)₂ /0.1 M TBAPF₆ MeCN solution. The potential was swept from 0.2 to −0.3 V at a scan rate of 10 mV/s with a 5 s period of chopped light (2.5 s light on and 2.5 s off). When the light was turned on, a rapid increase in the photoreduction current was observed, and when the light was turned off, the photocurrent rapidly dropped. However, there are current transients in both the light-on and the light-off regions in both cases falling off with time in 1 to 2 s to a steady-state value; this is a typical sign of surface recombination processes.^{16–19} The dark anodic current transient is also due to the reoxidation reaction of photogenerated EV⁺ to EV²⁺ at exposed Mo substrate or at impurities in the film, such as metallic CuSe. The presence of dark current at −0.15 to −0.3 V is also evidence of the existence of impurity zones. A pure crack-free p-type semiconductor should not exhibit any dark reduction current unless a high-negative overpotential is applied to overcome the Schottky barrier formed between p-type semiconductor and solution because of band bending. The measured photocurrent without any noticeable dark background current is around 0.65 mA/cm² at −0.13 V.

An ED-CIGS film was also prepared on a Mo substrate via the same method with NaCl, instead of LiCl, as the electrolyte and was examined by a PEC measurement. Figure 1b shows the LSV of this ED-CIGS film in 0.1 M EV(CIO₄)₂ and 0.1 M TBAPF₆ MeCN solution; the shape of the voltammogram is similar to that of the LiCl electrolyte film, but the photocurrent is higher (1.1 mA/cm² at −0.13 V) compared to the ED-CIGS film deposited in the LiCl electrolyte. The reoxidation current spike at the light-off point also became higher. This is caused by the EV⁺ produced by light irradiation being higher, so more EV⁺ can be reoxidized. This is evidence that the anodic current spike is due not only to surface recombination but also from dark reoxidation at any exposed electrode or metallic impurity

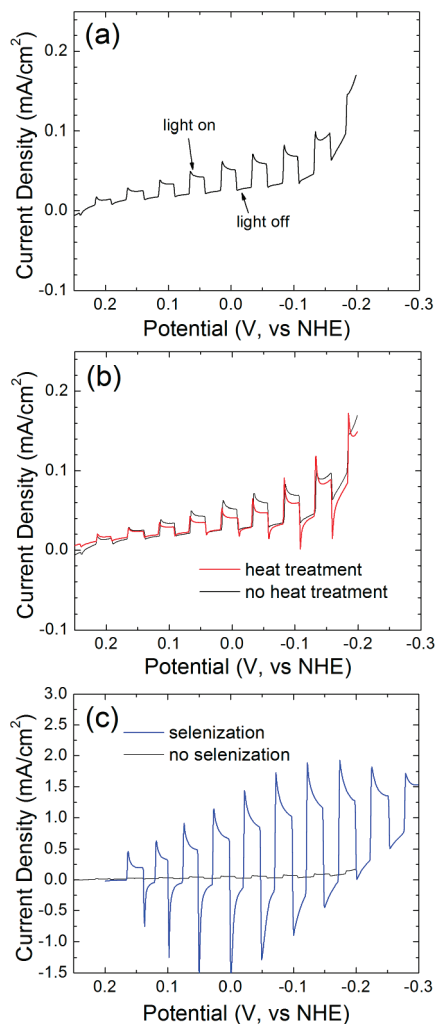


Figure 2. LSVs of NP-CIS films on Mo before heat treatment (a) and after heat treatment under vacuum at 250 °C (b) and under a Se atmosphere at 550 °C (c) with light chopping in 0.1 M $\text{EV}(\text{ClO}_4)_2$ and 0.1 M TBAPF_6 in MeCN. Scan rate: 10 mV/s, light source: Xe lamp (ca. 100 mW/cm²). LSV in a is also shown in b and c for comparison as a black line.

in the CIGS film. The reason for the improved photocurrent of the CIGS film deposited from NaCl electrolyte solution compared to that from the LiCl electrolyte solution is not clear. Although the benefit of Na on CIGS performance is widely accepted and many explanations have been proposed for this effect on thermally evaporated CIGS, there is no confirmed mechanism about the Na effect on CIGS.²⁰ More interestingly, the Na effect here was caused by Na^+ from the electrolyte solution while most of the other Na effects resulted from the Na content of a soda lime glass substrate that diffused into the CIGS films during thermal evaporation. Here, both CIGS films were prepared on glass substrates that contain Na.

An NP-CIS film prepared on Mo by spray coating was also tested. Figure 2a shows LSV of NP-CIS film in 0.1 M $\text{EV}(\text{ClO}_4)_2$ and 0.1 M TBAPF_6 MeCN solution with light chopping at a scan rate of 10 mV/s. While the shape of the voltammogram is similar to those of the ED-CIGS films, the photocurrent was significantly smaller (ca. 0.05 mA/cm² at -0.13 V) because the NP-CIS film had not been annealed and the particle size was only 14 nm as measured by transmission electron microscopy (TEM)⁵ with an oleylamine capping ligand on the particle surface. This probably induced more recombination on the surface of the film and at the grain boundaries. To

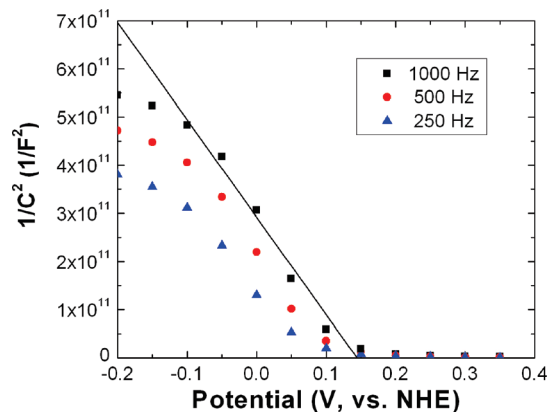


Figure 3. Mott–Schottky plots for NP-CIS film on Au substrate in 0.1 M TBAPF_6 in the dark. Plots were recorded at 1000 Hz (black squares), 500 Hz (red circles), and 250 Hz (blue triangles) with an AC amplitude of 10 mV at each potential. The line was drawn using 1000 Hz data at -0.10 to 0.15 V.

improve the photoefficiency of the NP-CIS films by increasing the grain size and removing the capping ligands, various postheat treatments were tried, and the resulting films were tested by the PEC method. Figure 2b shows the PEC result of NP-CIS film treated at 250 °C in vacuum. There was no improvement in the photocurrent compared to the film without heat treatment (black line in Figure 2b). Similarly, other heat treatments such as under air, Ar, or H_2 do not show any improvement except for heat treatment under a Se atmosphere (selenization). Figure 2c shows the LSV of NP-CIS film on Mo after selenization at 550 °C. The photocurrent of this film increased over 10 times at -0.13 V. This treatment promoted grain growth and removal of organic capping ligands. However, using this film to fabricate a solid-state device was challenging because the selenization process made the film rough and porous so that it was hard to prepare the top layers (CdS and ZnO) properly. However, the roughness had less of an effect in the liquid phase contact PEC cell.

Mott–Schottky Plots. The flat band potential of the NP-CIS films was determined from Mott–Schottky (MS) measurements carried out by EIS. Figure 3 shows MS plots ($1/C^2$ vs potential, where C is the capacitance of the semiconductor) of the NP-CIS film on Mo at different frequencies (250, 500, and 1000 Hz). The experiments were carried out in 0.1 M TBAPF_6 MeCN solution in the dark. The slope of the MS plots is negative confirming that the NP-CIS film is p-type. The flat band potential was found to be 0.15 V (vs NHE) from the x -intercept of the line drawn using data in the range from -0.10 to 0.15 V. The flat band potential measured here is comparable to those estimated from the photocurrent onset potentials of the LSVs.

CdS Layer Effect. PEC measurements were performed after thin (several nm) CdS layer deposition on top of the CIS and CIGS films. The CdS layer is normally used as a buffer layer in CIGS solid state solar cell devices. Interestingly, CdS layer-covered CIS and CIGS films showed much higher photocurrents in the PEC measurements. Figure 4a shows LSV of an NP-CIS film with CdS layer deposited by chemical bath deposition (NP-CIS/CdS) in 0.1 M $\text{EV}(\text{ClO}_4)_2$ and 0.1 M TBAPF_6 MeCN solution. Compared to an NP-film without a CdS layer (Figure 2a), the photocurrent at -0.2 V showed a large increase (~100 times after subtraction of the dark current), and the dark reoxidation current at 0.1 to -0.2 V completely disappeared. This is because the thin n-CdS layers probably depressed recombination processes on the surface of the CIS film and even

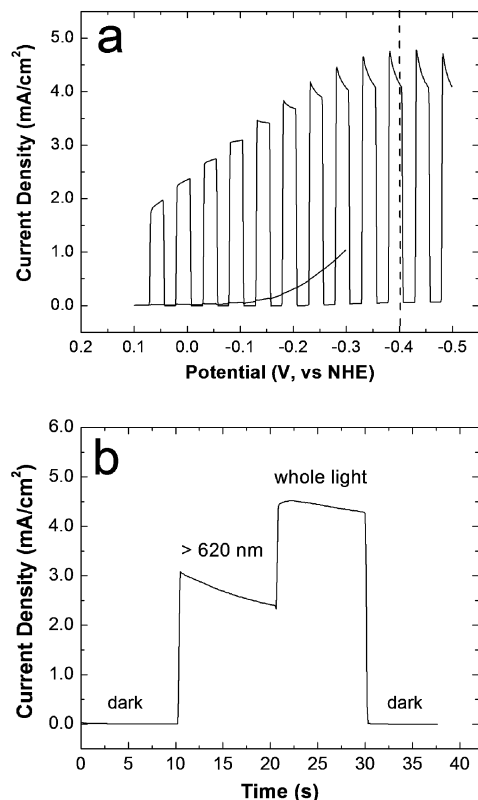


Figure 4. (a) LSVs of NP-CIS/CdS films on Au with light chopping in 0.1 M $\text{EV}(\text{ClO}_4)_2$ and 0.1 M TBAPF₆ in acetonitrile. Scan rate: 10 mV/s, light source: Xe lamp (ca. 100 mW/cm²). Dashed line indicates thermodynamic potential of EV reduction. Gray line is the LSV without CdS layer. Onset photocurrent potential is around 0.2 V which is not shown in the figure. (b) Current–time response curve of the same film at -0.4 V with dark, >620 nm, and whole light irradiation.

at the surface of the nanoparticles. Similar effects have been reported with CIS and CIGS films^{11,21} and other semiconductor materials.^{22,23} The CdS layer deposition also reduced the dark reduction of EV^{2+} in the negative potential region showing that this layer efficiently blocked the exposed Au substrate and metallic surface impurities. Additionally, the photocurrent at -0.4 V ($E_{1/2}$ for $\text{EV}^{2+/1+}$) was now comparable to the short-circuit current (J_{sc}) measured in a complete solid state device with a CuInSe_2 nanocrystal/CdS/ZnO working p–n junction.²⁴ An NP-CIGS/CdS film was also prepared and tested by the PEC measurement. The same effect of a CdS layer was observed for the CIGS-based films. While the film without treatment showed a small photocurrent, that of the NP-CIS/CdS film was much larger (Figure S2 in the Supporting Information).

Figure 4b shows the photocurrent–time response of an NP-CIS/CdS thin film on a Au substrate in 0.1 M $\text{EV}(\text{ClO}_4)_2/0.1$ M TBAPF₆ MeCN solution in the dark and with a 620 nm short wavelength cutoff filter and with total Xe lamp illumination at constant potential (-0.4 V vs NHE). To confirm that the photocurrent came from the CIS film and not from the CdS film, a 620 nm short wave cutoff filter was introduced. Since the band gap energy of the CdS is about 2.4 eV (515 nm), there was no light absorption by the CdS layer, and the photocurrent was still 60% of that under total light irradiation; the decrease in photocurrent simply results from a decrease in the light intensity, even at the longer wavelength, with the cutoff filter. This result confirms that the photoeffect originated from the CIS layer.

The higher photocurrent for NP-CIS films with CdS deposition allowed us to evaluate the effects of various treatments on

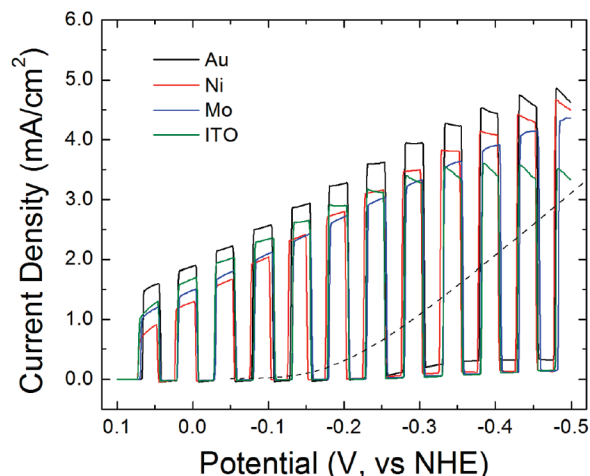


Figure 5. LSVs of NP-CIS/CdS films on Au, Ni, Mo, and ITO substrates with light chopping in 0.1 M $\text{EV}(\text{ClO}_4)_2$ and 0.1 M TBAPF₆ in MeCN. Scan rate: 10 mV/s, light source: Xe lamp (ca. 100 mW/cm²). Dashed line is LSV of bare Au substrate in same solution in dark. The LSVs of other substrates (Ni, Mo, and ITO) look similar.

the behavior of the films. For example, we prepared NP-CIS/CdS films on different substrates (Au, Mo, Ni, and ITO) and evaluated them with PEC measurements. Figure 5 shows the LSVs of NP-CIS/CdS films on the different substrates. The NP-CIS/CdS film on Au showed the highest photocurrent over all potential ranges, although the differences were not large. When we compare photocurrents at -0.4 V ($E_{1/2}$ of EV), which is equivalent to J_{sc} in the solid state device measurements, Au showed the highest photocurrent followed by Ni, Mo, and ITO. These results are comparable to the results observed in solid state device measurements (Figure S3 in the Supporting Information). Furthermore, the shape of voltammograms in the light-on condition can be qualitatively correlated with the fill factors obtained from solid state device measurements. We also tested NP-CIS/CdS films of different thickness. The thickness of the usual film was ~ 150 nm, and thicker films (up to ~ 600 nm) were prepared by extending the nanoparticle spray time. The results showed no improvement with thicker films, and in fact, there was a slight decrease of photocurrent with thickness (Figure S4 in the Supporting Information). This was also seen with the solid-state devices.²⁴ These results confirm that the PEC measurements can be used to evaluate properties of CIS films and to predict the properties of complete solid state devices.

The CdS layer was also deposited on the ED-CIGS film from the NaCl electrolyte (Figure 1b) to see if the same improvements were observed. Figure 6 shows the resulting LSV of ED-CIGS/CdS film in a 0.1 M $\text{EV}(\text{ClO}_4)_2/0.1$ M TBAPF₆ MeCN solution. The photocurrent increased after the CdS layer deposition over the whole potential range, but the improvement was not as dramatic as that found with the NP-CIS film (2.5 times photocurrent increase at -0.2 V vs ~ 100 times increase with NP-CIS). With the CdS layer, the NP-CIS film exhibited a higher photocurrent than the ED-CIGS film while the ED-CIGS film showed a much higher photocurrent than the NP-CIS film without a CdS layer. Furthermore, a dark current at relatively negative potential (-0.2 to -0.4 V) was still observed, although the magnitude decreased to some extent and the dark anodic spike also showed a higher current because of the higher production of EV^+ with the light on. These results suggest that the CdS layer did not block the exposed Mo substrate and the recombination process completely. This is probably due to the rough film morphology after selenization. Similar results were

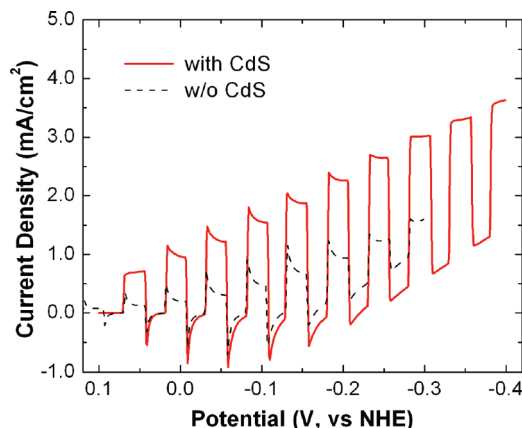


Figure 6. LSV of ED-CIGS/CdS film on Mo with light chopping in 0.1 M $\text{EV}(\text{ClO}_4)_2$ and 0.1 M TBAPF_6 in MeCN. The LSV of ED-CIGS film without CdS layer as shown in Figure 1b (dashed black line) is drawn for comparison. Scan rate: 10 mV/s, light source: Xe lamp (ca. 100 mW/cm^2).

observed on the selenized NP-CIS film after CdS deposition (Figure S5 in the Supporting Information). In fact, the solid-state device results with an ED-CIGS film not as efficient as the NP-CIS films without selenization probably because of difficulty in making top layers on rough surfaces, which may cause leakage currents.

LSVs of three films (NP-CIS, selenized NP-CIS, and ED-CIGS) with and without CdS films are compared in a single figure (Figure S6 in the Supporting Information).

Photoresponse Measurement in Aqueous Solution and IPCE. The NP-CIS/CdS film was also tested in aqueous solution. Here, instead of $\text{EV}(\text{ClO}_4)_2$, MVCl_2 was used as a

redox species and 0.1 M KCl was used as the electrolyte. Figure 7a shows the LSV of NP-CIS/CdS film on Au in aqueous solution. The shape of the voltammogram is similar to that with a MeCN solution. Figure 7b shows IPCE plots over the range of 400–900 nm calculated from eq 1

$$\text{IPCE}(\%) = 1240 \times (j_{\text{ph}}/\lambda \cdot P_{\text{in}}) \times 100 \quad (1)$$

where j_{ph} is the photocurrent density measured at -0.4 V versus NHE (mA/cm^2), λ is the wavelength (nm), and P_{in} is the incident light power density (mW/cm^2). The calculated IPCE values are near 20% in all wavelength regions where light is absorbed. Since this film was relatively thin (~ 150 nm), it did not absorb 100% of the incident light as shown by the absorbance spectrum of an NP-CIS film on glass (Figure 7c). From the measured absorbance, we calculated the absorbed photon to current conversion efficiencies (APCEs); these are plotted as a function of wavelength (Figure 7d). The resulting APCEs are around 40–70%. These values correspond well with what is observed in the solid state nanocrystalline devices with thin absorber layers.²⁵

Conclusions

We have demonstrated the PEC characterization of NP-CIS and ED-CIGS films by reduction of EV in MeCN and MV in aqueous solution. This simple PEC measurement can be used to evaluate the properties of the CIS and CIGS films without making full solid devices. This measurement was used to compare ED-CIGS films prepared in LiCl and NaCl electrolytes and to confirm selenization of NP-CIS film to improve its photo property.

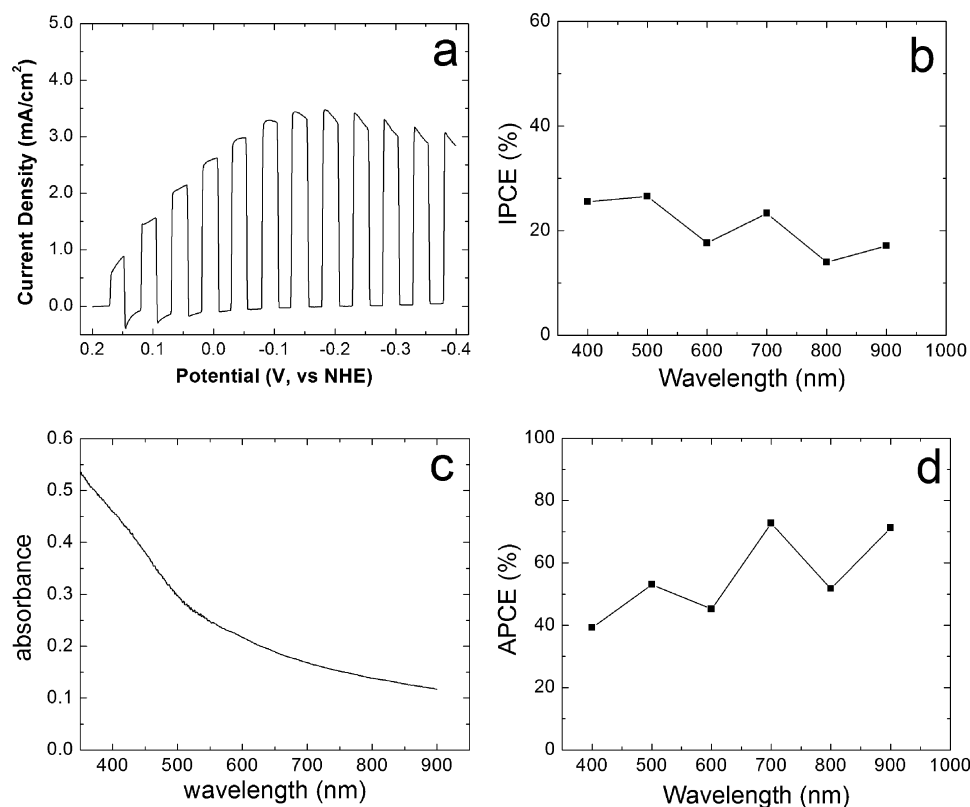


Figure 7. (a) LSVs of NP-CIS/CdS film on Au with light chopping in 0.1 M MVCl_2 and 0.1 M KCl aqueous solution. Scan rate: 10 mV/s, light source: Xe lamp (ca. 100 mW/cm^2). (b) IPCE plot of same film calculated from the photocurrents at -0.4 V. (c) Absorbance spectrum of NP-CIS film on glass. (d) APCE plots calculated from b and absorbed light c. Absorbed light was calculated by $1 - 10^{-A}$, where A is absorbance.

CdS layer deposition on the NP-CIS and ED-CIGS films produced greatly enhanced photocurrents for EV and MV reduction probably by suppressing recombination processes; for example, the NP-CIS/CdS film showed an almost 100 times photocurrent enhancement and the photocurrent at -0.4 V versus NHE was comparable to short-circuit current of solid-state devices prepared using a same film. EIS experiments and Mott–Schottky plots were used to measure the flat band potential of the NP-CIS films (-0.15 V vs NHE), and IPCE and APCE measurements of NP-CIS/CdS showed around 20% and 40–70%, respectively, in 0.1 M $\text{MVCl}_2/0.1$ M KCl aqueous solutions.

Acknowledgment. We acknowledge support from the Robert A. Welch Foundation (F-0021) and partial support from the Department of Energy (SISGR - DE-SC0002219). We acknowledge help of Dariya Reid with the synthesis of the nanocrystalline solutions.

Supporting Information Available: Additional experimental data figures. This material is available free of charge via the Internet at <http://pubs.acs.org>.

References and Notes

- (1) Kapur, V. K.; Bansal, A.; Le, P.; Asensio, O. I. *Thin Solid Films* **2003**, *431–432*, 53.
- (2) Kaelin, M.; Rudmann, D.; Kurdesau, F.; Meyer, T.; Zogg, H.; Tiwari, A. N. *Thin Solid Films* **2003**, *431–432*, 58.
- (3) Mitzi, D. B.; Yuan, M.; Liu, W.; Kellock, A. J.; Chey, S. J.; Deline, V.; Schrott, A. G. *Adv. Mater.* **2008**, *20*, 3657.
- (4) Liu, W.; Mitzi, D. B.; Yuan, M.; Kellock, A. J.; Chey, S. J.; Gunawan, O. *Chem. Mater.* **2010**, *22*, 1010.
- (5) Panthani, M. G.; Akhavan, V.; Goodfellow, B.; Schmidtke, J. P.; Dunn, L.; Dodabalapur, A.; Barbara, P. F.; Korgel, B. A. *J. Am. Chem. Soc.* **2008**, *130*, 16770.
- (6) Guo, Q.; Kim, S. J.; Kar, M.; Shafarman, W. N.; Birkmire, R. W.; Stach, E. A.; Agrawal, R.; Hillhouse, H. W. *Nano Lett.* **2008**, *8*, 2982.
- (7) Valderrama, R. C.; Sebastian, P. J.; Enriquez, J. P.; Gamboa, S. A. *Sol. Energy Mater. Sol. Cells* **2005**, *88*, 145.
- (8) Djellal, L.; Bouguelia, A.; Hanifi, M. K.; Trari, M. *Sol. Energy Mater. Sol. Cells* **2008**, *92*, 594.
- (9) Djellal, L.; Omeiri, S.; Bouguelia, A.; Trari, M. *J. Alloys Compd.* **2009**, *476*, 584.
- (10) Neumann, B.; Bogdanoff, P.; Tributsch, H. *J. Phys. Chem. C* **2009**, *113*, 20980.
- (11) Yokoyama, D.; Minigishi, T.; Maeda, K.; Katayama, M.; Kubota, J.; Yamada, A.; Konagai, M.; Domen, K. *Electrochem. Commun.* **2010**, *12*, 851.
- (12) Calixto, M. E.; Dobson, K. D.; McCandless, B. E.; Birkmire, R. W. *J. Electrochem. Soc.* **2006**, *153*, G521.
- (13) Kannan, R.; Miguel, A. C.; Craig, L. P.; Sally, A.; Falah, S. H.; James, K.; David, Y.; Manuel, R.; Wyatt, M.; Rommel, N.; James, W.; Anna, D. *Prog. Photovoltaics: Res. Appl.* **2003**, *11*, 225.
- (14) McCandless, B. E.; Shafarman, W. N. Chemical Surface Deposition of Ultra-Thin Semiconductors. U.S. Patent 6,537,845, March 25, 2003.
- (15) *Encyclopedia of Electrochemistry-Semiconductor Electrodes and Photoelectrochemistry*; Licht, S., Ed.; Wiley-VCH: Weinheim, Germany, 2002; Vol. 6.
- (16) Peter, L. M. *Chem. Rev.* **1990**, *90*, 753.
- (17) Hagfeldt, A.; Lindstrom, H.; Sodergren, S.; Lindquist, S.-E. *J. Electroanal. Chem.* **1995**, *381*, 39.
- (18) Beranek, R.; Kisch, H. *Electrochem. Commun.* **2007**, *9*, 761.
- (19) Radecka, M.; Rekas, M.; Trenczek-Zajac, A.; Zakrzewska, K. *J. Power Sources* **2008**, *181*, 46.
- (20) Rockett, A. *Thin Solid Films* **2005**, *480–481*, 2.
- (21) Shirakata, S.; Ohkubo, K.; Ishii, Y.; Nakada, T. *Sol. Energy Mater. Sol. Cells* **2009**, *93*, 988.
- (22) Long, M.; Cai, W.; Kisch, H. *J. Phys. Chem. C* **2008**, *112*, 548.
- (23) Kim, H. G.; Borse, P. H.; Choi, W.; Lee, J. S. *Angew. Chem., Int. Ed.* **2005**, *44*, 4585.
- (24) Akhavan, V. A.; Goodfellow, B. W.; Panthani, M. G.; Reid, D. K.; Hellebusch, D. J.; Adachi, T.; Korgel, B. A. *Energy Environ. Sci.* **2010**, *3*, 1600.
- (25) Akhavan, V. A.; Panthani, M. G.; Goodfellow, B. W.; Reid, D. K.; Korgel, B. A. *Energy Express* **2010**, *18*, A411.

JP108170G